2016

Oxidative durability of TBCs on Ti_2AlC MAX phase substrates

James L. Smialek
NASA Glenn Research Center, james.l.smialek@nasa.gov

Bryan J. Harder
NASA Glenn Research Center

Anita Garg
NASA Glenn Research Center

Surface & Coatings Technology 285 (2016) 77–86

Contents lists available at ScienceDirect

Surface & Coatings Technology

journal homepage: www.elsevier.com/locate/surfcoat

Oxidative durability of TBCs on Ti_2AlC MAX phase substrates

James L. Smialek *, Bryan J. Harder, Anita Garg

NASA Glenn Research Center, Cleveland, OH 44135, United States

ARTICLE INFO

Article history:
Received 8 September 2015
Revised 10 November 2015
Accepted in revised form 13 November 2015
Available online 14 November 2015

Keywords:
MAX phases
Thermal barrier coatings
Oxidation
Spallation
Alumna scales

ABSTRACT

Air plasma spray (APS) and plasma-spray-physical vapor deposition (PS-PVD) yttria-stabilized zirconia (YSZ) thermal barrier coatings (TBC), ~80–100 μm thick, were produced on a commercial Ti_2AlC MAX phase compound. They were oxidized in interrupted furnace tests for 500 h each, at five successive temperatures from 1100°–1300 °C. The APS coating survived 2400 accumulated hours, failing catastrophically after 500 h at 1300 °C. Porosity, large cracks, sintering, and high monoclinic YSZ phase contents were seen as primary degradation factors. The PS-PVD coating remained completely intact over 2500 total hours (65 cycles) including 500 h at 1300 °C, exhibiting only fine porosity and microcracking, with less monoclinic. These Ti_2AlC systems achieved a minimum α-Al_2O_3 scale thickness of 29 and 35 μm, respectively, as compared to ~6 ± 2 μm on average at failure for conventional bond coats on superalloys. Accordingly, times predicted from thermogravimetric analyses (TGA) of oxidation kinetics project an improvement factor of ~25–50× for the time to achieve these scale thicknesses at a given temperature. Extreme oxidative TBC durability is achieved because the thermal expansion coefficient of Ti_2AlC is only slightly different than those for α-Al_2O_3 and YSZ. The strain energy term driving scale and TBC failure is therefore believed to be fundamentally diminished from the large compressive stress produced by higher expansion superalloys.

Published by Elsevier B.V.

1. Introduction

MAX phases (M = early transition metal, A = Al, Si, Ga, Ge, etc., X = C, N) have been studied intensely because of their unique properties of thermal stability, thermal shock resistance, and damage tolerance derived from a special intercalated crystal structure [1]. Alumina-forming MAX phases (Ti_3AlC_2, Ti_2AlC, and Cr_2AlC) are very oxidation resistant while remaining stable to temperatures on the order of 1400 °C [2,3,4,5,6,7,8]. A number of in-depth oxidation studies (as reviewed and analyzed by Tallman et al. [2]) have established slow growing alumina kinetics similar to oxidation resistant metallic FeCrAl-type heater alloys. Due to grain growth in the scale, the kinetics follow a cubic rate law, except for an initial transient due to rapid TiO_2 growth on the order of just 5 min [2,7,9,10]. Furthermore, growth models produce grain boundary diffusion rates in the scale in accord with those obtained for oxidation resistant alumina-forming FeCrAl alloys [3,9,10,11].

Another beneficial oxidation attribute of the Ti_2AlC MAX phase is the relatively low coefficient of thermal expansion (α_{CTE}) in comparison to metallic alumina-formers [4]. Published at 8.2×10^{-6}/°C, [8,12] it is a much closer match to that of α-Al_2O_3 (9.3×10^{-6}/°C), as compared to most Ni–Al base alloys having $15–16 \times 10^{-6}$/°C. Those metal systems produce high compressive stresses in the scale upon cool down which are believed to drive scale spallation. To that point, excellent scale adherence and cyclic oxidation resistance have been reported for Ti_2AlC [3,4,6]. Furthermore, numerous studies have produced relatively thick scales during high temperature oxidation of Ti_2AlC, but none reports any loss of scale upon cooling.

Thermal barrier coatings have been the subject of intense research for many years due to their successful incorporation into turbine engine components, primarily film-cooled blades and vanes. Here classic examples would be APS (or EB-PVD) 7YSZ TBC on a NiCoCrAlY (or Ni(Pt)Al) bond coat, for 2nd generation single crystal Ni-base superalloy airfoils. The purpose of the bond coat is to prevent oxidation of the substrate and provide a slowly oxidizing, stable interface to bond with the YSZ. Failure mechanisms typically address oxidation of the bond coat as an important factor, incorporating other cyclic instabilities such as interfacial spallation, ratcheting, and rumpling of the bond coat surface. These will not be addressed in detail here, but are in part related to interdiffusion with the substrate, phase transformations, and grain boundary ridges in the coating. While numerous studies have attempted process improvements to address these issues, it can be said that TBC failure generally occurs before the scale reaches ~10 μm, amounting to less than ~1000 hot hours of cyclic oxidation at 1150 °C [15].

However more substantial improvements are realized for atypical substrates, such as doped NiAl(Zr, Cr, Si, Hf) and FeCrAl(X) [16–19]. While these do not have the mechanical properties of superalloys, they illustrate significantly improved oxidative TBC lives produced by eliminating problematic interactions between substrates and bond coats. However these metallic alumina-formers still maintain α_{CTE} in the

* Corresponding author.
E-mail address: James.L.Smialek@nasa.gov (J.L. Smialek).

http://dx.doi.org/10.1016/j.surfcoat.2015.11.018
0257-8972/Published by Elsevier B.V.

range of 15–18 × 10^{-6}/°C and produce severe compressive stresses on the scale and TBC. The close α_{CTE} match of Ti_2AlC with α-Al_2O_3 and YSZ is thus expected to decrease a primary cause of failure, albeit with substantial scale growth still occurring at the rate of most alumina-formers.

Thus the purpose of the present preliminary study is to demonstrate the oxidative durability of YSZ thermal barrier coatings on Ti_2AlC MAX phase samples, having the advantage of thermal expansion matching, scale adhesion, and no interactions with superalloy substrates. To this end, APS and PS-PVD coatings were examined in interrupted furnace tests, stepped from 1000 °C to 1300 °C. Another intent is to determine the range of scale thickness that can be tolerated in the absence of the other detrimental or diminishing factors mentioned above.

2. Experimental

Ti_2AlC MAX phase ingots were obtained from Kanthal/Sandvik and machined into ~2 × 15 × 20 mm coupons. These were polished through 600 grit emery and lightly grit blast with 200 mesh alumina. One coupon was coated with about 100 μm of commercial Zircoa 8YSZ powder using conventional air plasma spray (APS, Oerikon Metco) at the NASA Glenn Research Center. The plasma torch was run at 40 kW using Ar/N_2. The standoff distance was ~100 mm and the samples were preheated by passing the torch across the samples twice before starting deposition.

A second sample was coated with about 80 μm of commercial 8YSZ powder using low pressure, plasma spray-physical vapor deposition (PS-PVD, Sulzer-Oerlikon Metco) also at NASA Glenn Research Center. PS-PVD is a unique processing method that combines conventional thermal spray and vapor phase methods, enabling deposition of coatings via the liquid phase or the vapor phase. The PS-PVD coatings processed for this study were deposited mostly via the vapor phase, which resulted in a columnar-like microstructure similar to traditional EB-PVD methods. Samples were coated normal to the torch at a standoff distance of 1.68 m. The torch power was 94 kW, plasma gases were 40/80 slpm Ar/He, and the feedstock powder was Metco 6700 7YSZ. Coatings were deposited at 150 Pa (1.13 Torr), for 16 min.

Samples were intermittently oxidized in a box furnace (Rapid Temp) at progressively increasing temperatures in an attempt to determine a maximum survivable temperature. (The first low temperature proof exposure was only for 50 h at 1000 °C). Subsequently, the samples were exposed for 500 h each at 1100°, 1150°, 1200°, 1250° and 1300 °C, successively. The time intervals for bench-top cooling in ambient air and weighing followed a graduated sequence, at approximately: 1, 2, 5, 10, 15, 20, 50, 100, 200, 300, 400, and 500 h for each temperature. (Consequently, the designation of test time at any one temperature implies completion of all previous exposures at lower temperatures). Optical and scanning electron microscopy (15 kV, carbon coated) was used to characterize substrate, scale, and coating structure, damage and spallation. Separate cross-sections were obtained after the 1200 °C and 1300 °C sequences were completed. XRD diffractometer scans were used to identify substrate, scale, and coating phases after testing was completed (Brüker). Some estimates of the monoclinic zirconia phase content were made using a Rietveld refinement analysis with Jade software. Coefficient of thermal expansion was measured on ~-2 mm × 2 mm × 20 mm strips from 25 to 1300 °C, at 10 °C/min heating in Ar using a Netsch 402C dilatometer.

3. Results

3.1. Mass change and coating durability

Fig. 1 indicates the oxidative mass gain for the APS TBC on the Ti_2AlC MAX phase substrate. (No degradation was observed after just 50 h of proof testing at the initial low temperature, 1000 °C). Accordingly, samples were oxidized successively from 1100 °C–1300 °C for 500 h at each temperature. Interrupted tests produced no visible damage, each successively at 1100°, 1150°, 1200°, and 1250 °C. Only a regular increase

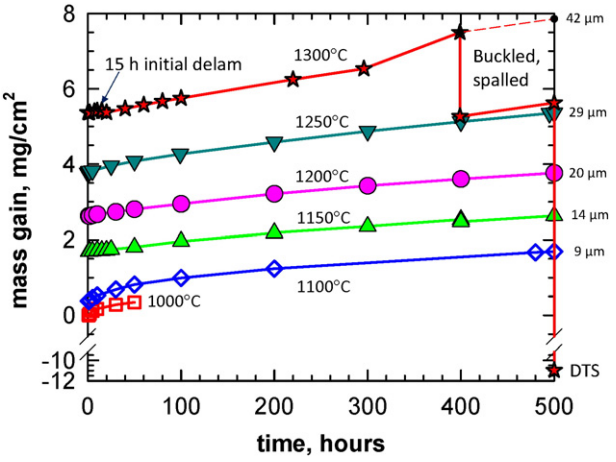

Fig. 1. Oxidative mass gain of APS YSZ TBC on Ti_2AlC MAX phase substrate for successive exposures at 1000–1300 °C. (Corresponding scale thickness estimates indicated for each 500 h, interrupted test).

in mass gain occurred due to oxidation of the substrate. After 1 and 15 h at 1300 °C (1 and 5 cycles), some initial edge damage, a slight mass change irregularity, and initial delamination (discussed later) was observed. The majority of the coating remained intact until 400 h at 1300 °C, when more coating buckling occurred along with mass loss. At 500 h, the coating was only partially attached to the substrate after cooling, then completely detached overnight under ambient room conditions. The spalled coating remained intact as one large flake, more typical of APS delamination failures, and did not spontaneously disintegrate into fine particles. This final spallation event resulted in a net mass loss of −11 mg/cm^2 (YSZ) after sustaining a maximum mass gain of ~7.5 mg/cm^2 (TGO) after 400 h at 1300 °C. The projected mass gain would have been ~7.8 mg/cm^2 if no coating spallation occurred. Assuming primarily α-Al_2O_3 scales, the mass gains suggest scales 29 μm thick at the earliest observation of edge damage and 42 μm after the entire test. For comparison purposes, it can be said that the accumulated hot time reached 2450 h before appreciable coating loss.

Similarly, Fig. 2 indicates the oxidative mass gain for the PS-PVD TBC on the Ti_2AlC MAX phase substrate. Again, no degradation was observed at the initial low temperature (1000 °C), and the same longer duration test sequence was performed at successively increasing temperatures. As with the APS coating, successive 500 h interrupted tests produced no visible damage at 1100°, 1150°, 1200°, 1250 °C, and now at 1300 °C

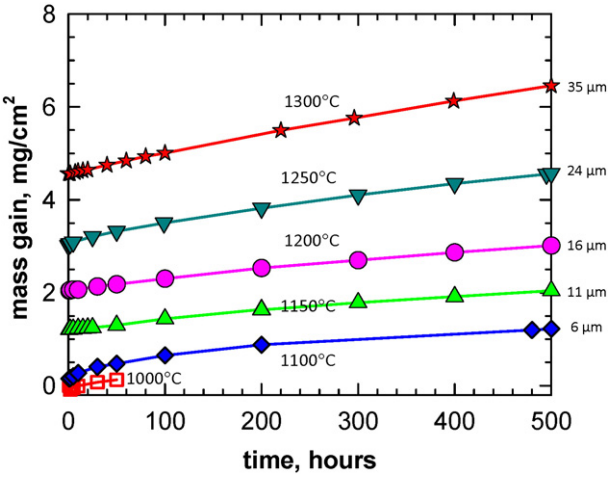

Fig. 2. Oxidative mass gain of PS-PVD YSZ TBC on Ti2AlC MAX phase substrate for successive exposures at 1000–1300 °C. (Corresponding scale thickness estimates indicated for each 500 h, interrupted test).

as well. Initial testing may have produced slight coating loss at edge processing defects, partially responsible for the lower overall mass curves. There is some microstructural indication (below) that less TiO_2 transient oxides formed, also resulting in lower mass gains. The majority of the coating remained intact through the completion of the test after 500 h at 1300 °C. This final exposure resulted in a net mass gain of ~6.5 mg/cm^2. Assuming primarily α-Al_2O_3 scales, the mass gains suggest scales 35 μm thick after the entire test. For comparison purposes, it can be said that the total accrued hot time durability was 2550 h with no appreciable coating damage.

3.2. Coating appearance and microstructure

The appearance of the coatings after completion of the 1200 °C test series is provided in Fig. 3. Very little change has occurred from the very beginning of furnace testing. A slight edge delamination was noted for the as-processed APS coating, and local TBC absences can be seen for the PS-PVD coating. The latter also exhibited numerous small 'spit' defects on the major surface where improper hillock deposition defects did not adhere initially or were partially removed during cycling.

3.2.1. APS YSZ on Ti_2AlC

The partial coating failure for the APS coating at 1300 °C can be seen just before the cycle where substantial mass loss was measured, Fig. 4. Edge delamination (a) and buckling (b) are readily apparent, but still relatively localized to one corner of the sample where the initial processing defect had been observed.

Although failure had initiated earlier, the APS sample test was continued until the 500 h test sequence was finished. The SEM/BSE images in Fig. 5a and b are representative of the major sample surface after total delamination. The bright areas are a mixture of YSZ and YZTA-modified interface phases (i.e., Y–Zr–Ti–Al oxide reaction phase discussed below). The dark areas are primarily Al_2O_3. It is interesting to point out that the grain sizes of all three scale, coating, and reaction product oxides are on the order of 2–8 μm, albeit with considerable variation. Smaller <1 μm grain boundary precipitates of Ti-rich oxides, noted on the exposed Al_2O_3 grains, did not appear to be part of the YSZ topcoat.

The microstructure of an epoxy mounted and polished slice of an APS sample sectioned after 500 h testing at 1200 °C is presented in Fig. 6. The 100 μm YSZ coating (a) is seen to be essentially intact, though replete with cracks and porosity. There is little evidence of initial strain tolerant splat boundaries characteristic of APS coatings. An adherent 20 μm Al_2O_3 scale (b) is apparent at the YSZ–Ti_2AlC interface. Higher magnification (c) reveals regions where considerable amounts of TiO_2 remained, presumably from the initial transient outer scales where this oxide is known to predominate. Scale thicknesses were roughly similar on the uncoated back side, here and in the subsequent 1300 °C sections. Substantial amounts of YSZ–TiO_2–Al_2O_3 reacted particles exist at the interface in the vicinity of TiO_2, as well as within YSZ itself. The EDS spectra (d) were essentially the same as those obtained in plan view (ref. Fig. 5). Intensities were converted to mole %, using the EDS standardless correction program. This yielded 8.2Al–14.4Ti–12.7Y–14.2Zr–50.6O (mole %), only roughly equivalent to $2Al_2O_3 \cdot 3Y_2O_3 \cdot 7ZrO_2 \cdot 7TiO_2$, with oxygen somewhat below that needed for this stoichiometry (~64%).

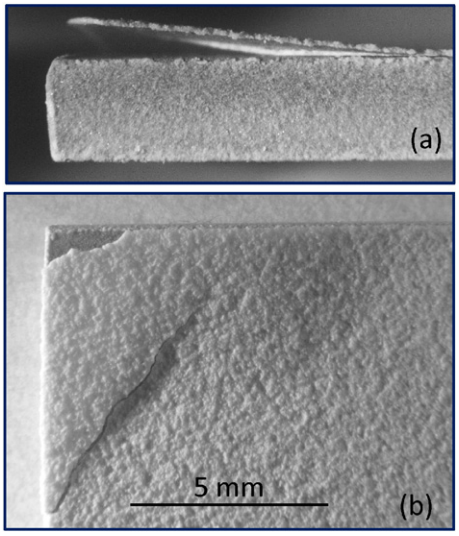

Fig. 4. APS YSZ coating edge delamination (a) and surface buckling (b) after 300 h oxidation at 1300 °C. (1850 total hours and ~56 cycles). Edge and plan views, 7.5×.

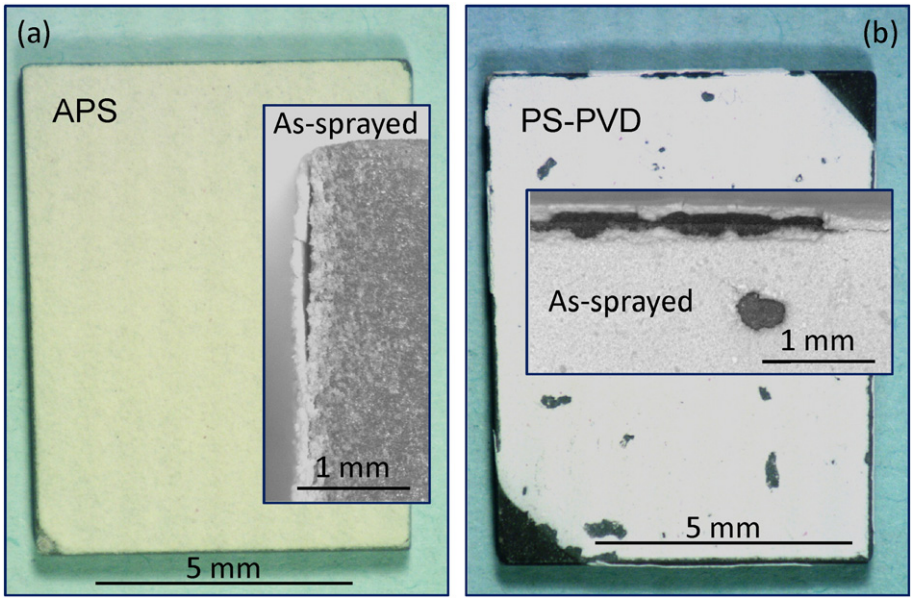

Fig. 3. Macrophotos of intact APS and PS-PVD YSZ coatings on Ti_2AlC substrates after 500 h oxidation at 1200 °C. (1550 total hours; ~45 cycles). Insets show processing edge defects before testing, 7.5×.

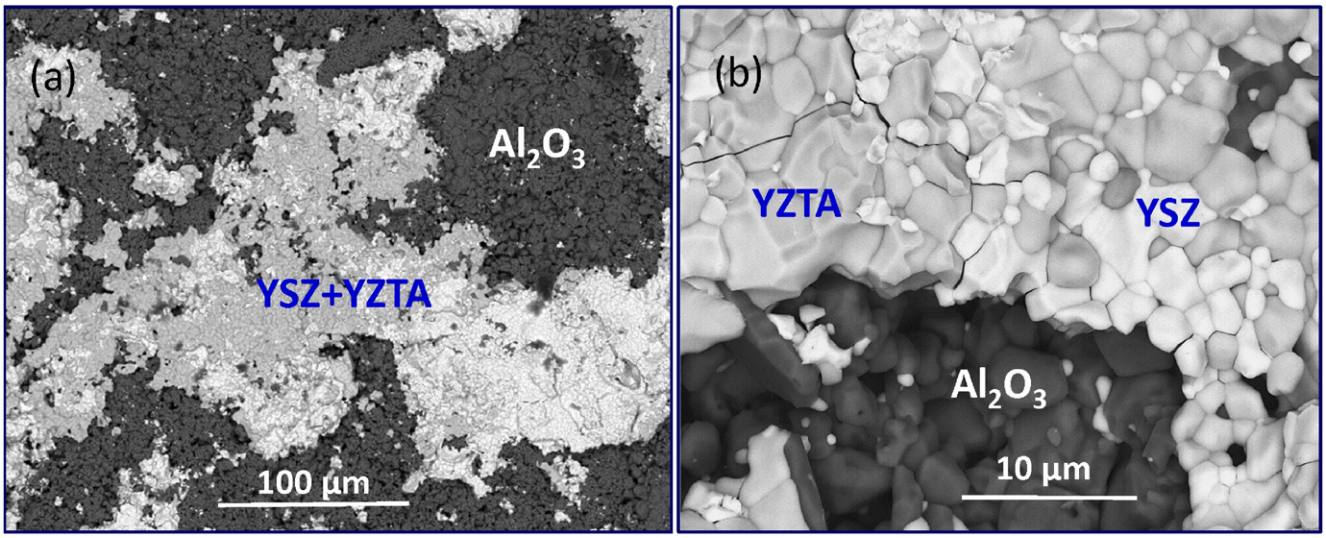

Fig. 5. Mixed failure structure for APS YSZ coating on Ti_2AlC substrate after 500 h at 1300 °C (SEM/BSE). (a) Overview showing bright YSZ features and dark oxidized substrate. (b) Exposed Al_2O_3 scale and details of various YSZ and YZTA grains in the fractured TBC after failure.

Numerous interfacial pores and microcracks in the YSZ were apparent. Note that the next cycle (1300 °C, 1 h) initiated some minor coating failure, though full progression of failure required hundreds of hours more. After failure, test completion at 500 h, and subsequent sectioning, the scale can be seen to be ~37–40 µm in Fig. 7, becoming somewhat irregular at higher temperatures. Some differences are then noted from cross section measurements and those converted from mass gains, as indicated on Figs. 1 and 2. The Ti-rich reaction zones did not thicken appreciably. There is little YSZ topcoat left, on the order of perhaps 10 µm in places, with another few µm of TiO_2–YSZ reaction phases.

3.2.2. PS-PVD YSZ on Ti_2AlC

The surface of the PS-PVD coating at the completion of the test is shown in Fig. 8. While the majority of the coating remained intact, scattered 1 mm bare regions (Fig. 8a) indicated initial process defects that either began uncoated or were prone to local spallation. Linear chains of valleys or hillocks also suggest some anomalous non-uniformity. Fig. 8b exhibits the fine 20 µm nodular structure of the PS-PVD coating, each composed of hundreds of finer 1–5 µm grains, Fig. 8c. The ledge of the TBC adjacent to the defect is shown in Fig. 8d. Here a network of intergranular and transgranular microcracks can be

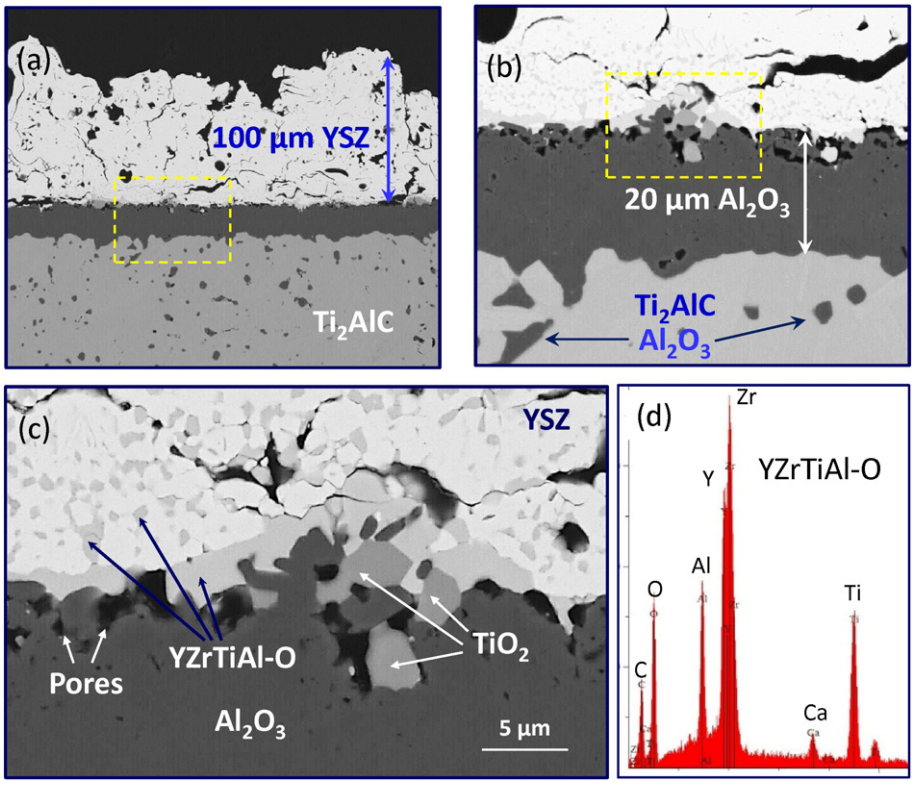

Fig. 6. Cross-section of APS YSZ–Ti_2AlC interface after 500 h testing at 1200 °C (SEM/BSE). a) Low magnification showing 100 µm APS coating; b) intermediate magnification of (a) showing well-bonded 20 µm Al_2O_3 scale on and Al_2O_3 particles in the MAX phase substrate; c) higher magnification of (b) showing interfacial porosity, residual surface TiO_2 scale, reacted YSZ–TiO_2–Al_2O_3 particles at interface and within YSZ; and d) corresponding point EDS spectra of these particles with high Y, Zr, Ti, and Al peaks.

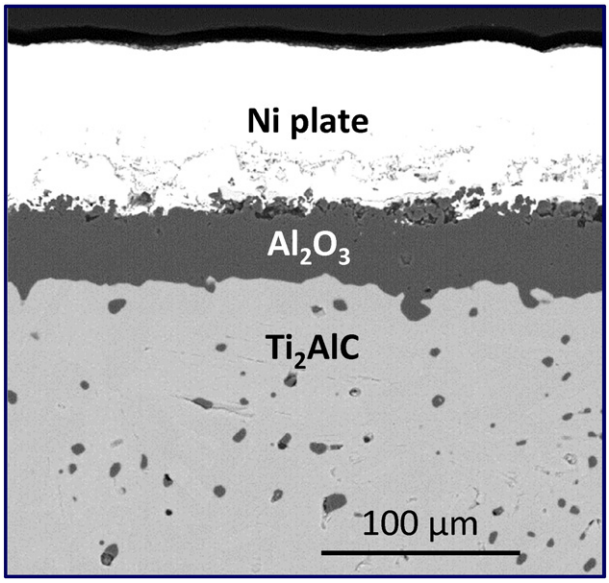

Fig. 7. Cross-section of APS YSZ–Ti_2AlC interface after 500 h testing at 1300 °C (SEM/BSE). Overview shows little YSZ coating remaining, but intact 37–40 μm Al_2O_3 scale.

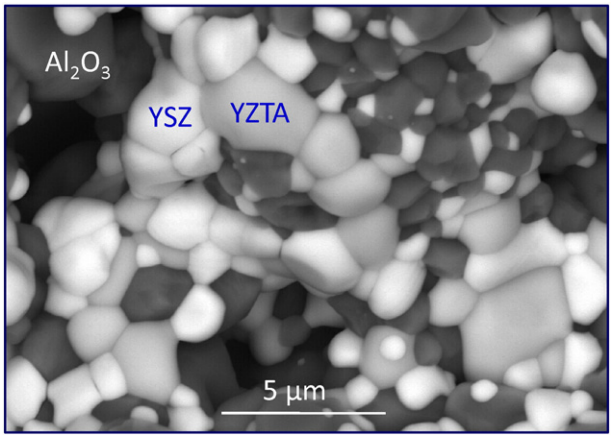

Fig. 9. Exposed Ti_2AlC substrate after testing PS-PVD coating for 500 h at 1300 °C. Al_2O_3 scale and included grains of YSZ, YZTA, and (Ti, Zr) oxides.

seen traversing the ledge, sometimes arresting within a grain or at a grain boundary. The defect regions without coating, Fig. 9, exhibited exposed Al_2O_3 grains and Y, Zr, Ti, Al-rich oxide grains, similar to features discussed for the APS coating. Also present were similar oxide grains with just Zr and Ti primary cation components, in variable amounts.

The cross-section of the PS-PVD sample sectioned after 500 h testing at 1200 °C is presented in Fig. 10. The 80 μm YSZ coating is seen to be intact and relatively uncracked and devoid of splat boundaries. It is replete with limited micro- or finer porosity, characteristic of these coatings. The quasi-columnar structure, correlating with the nodules observed in plan view (Fig. 8) is reflective of the dendritic or columnar growth characteristic of EB-PVD coatings, and PS-PVD structures have been discussed at length in this regard [20,21]. Again, an adherent 20 μm Al_2O_3 scale is apparent at the YSZ–Ti_2AlC interface, but TiO_2 was not observed in the fields examined. Some very fine (Y, Zr, Ti, Al, O) reacted particles existed within the Al_2O_3 scale near the YSZ interface, but could not be easily resolved in the YSZ itself. However, reacted particles were clearly present in the defective areas (Fig. 9), similar to those seen for the APS spalled surface, but to a lesser degree. The minimal amount of interface damage and fine, entrained porosity allowed this sample to survive the next two test series at 1250° and 1300 °C for the full 500 h, with no apparent macroscopic damage.

The PS-PVD scale thickness after the 1200 °C series was ~20 μm and the same as that on the APS sample. It may be likely that any difference in weight change between the APS and PS-PVD samples was only due to minor coating losses rather than substantive scale growth differences.

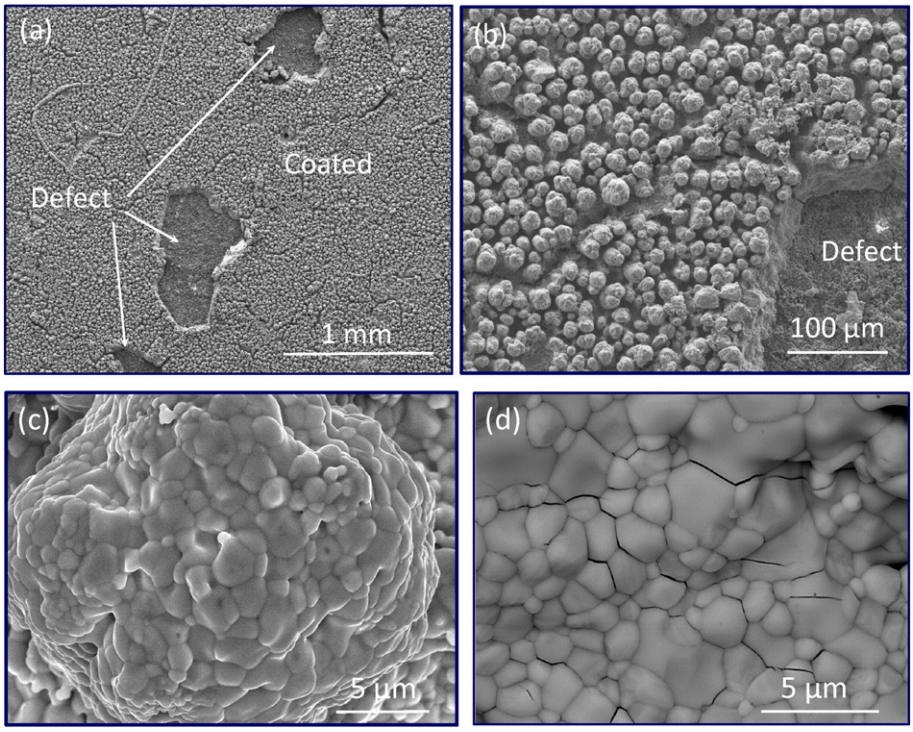

Fig. 8. Overview of PS-PVD coating after 500 h at 1300 °C (SEM/BSE). (a) Intact nodular surface and defected bare areas; (b) nodular surface structure of dendritic column; (c) ~1–3 μm grains on YSZ nodule mound; and (d) ~1–3 μm grains in YSZ vertical ledge adjacent to defect area.

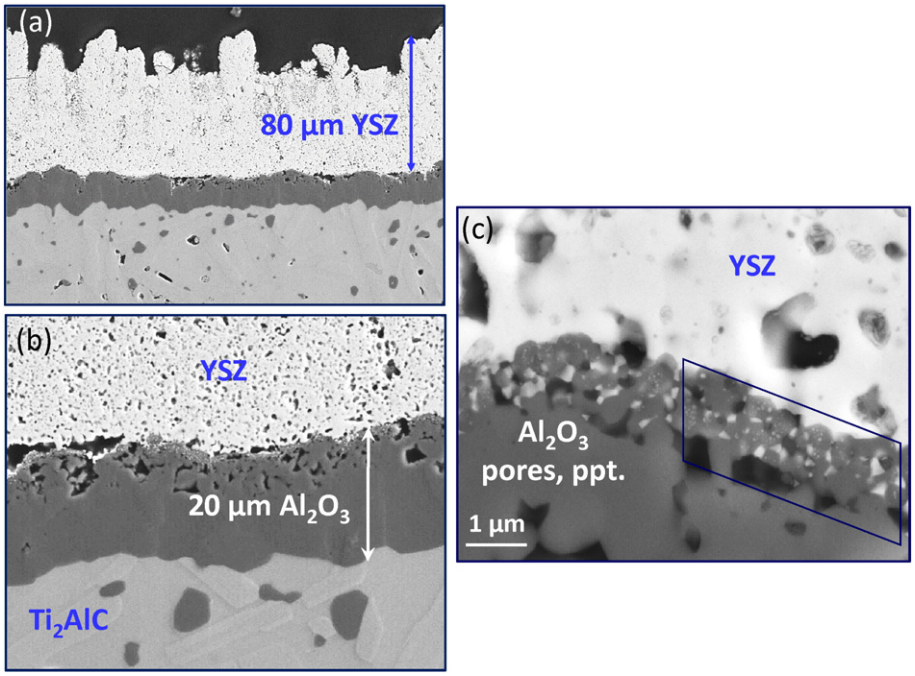

Fig. 10. Cross-section of PS-PVD YSZ-Ti_2AlC interface after 500 h testing at 1200 °C (SEM/BSE). a) Low magnification showing 80 µm APS coating; b) intermediate magnification of (a) showing well-bonded 20 µm Al_2O_3 scale on and Al_2O_3 particles in the MAX phase substrate, with coarse interface porosity; and c) higher magnification of (b) showing fine pores in YSZ and reacted YSZ–TiO_2–Al_2O_3 particles at the interface.

The scale thickness after 500 h at 1300 °C can be seen to be ~32–37 µm in the cross section of Fig. 11a, with little overall change from 1200 °C. A fine distribution of lateral cracks in the YSZ is also apparent, Fig. 11b, often terminating at the fine porosity features. This may reflect a more strain tolerant coating than the APS structure.

3.2.3. XRD results

XRD analyses of the YSZ coatings identified t′ tetragonal as the primary coating phase in both systems. Rietveld analyses revealed ~12.1% monoclinic in the as-sprayed APS coating, changing little at 1100 °C. However the monoclinic increased substantially after higher temperature exposures, finishing at a very high 62.1% (with 9.3% cubic) after 500 h testing at 1300 °C. In comparison, the PS-PVD coating had 1.6% monoclinic after 1100 °C, finishing at 27.8% at the end of 1300 °C, 500 h testing. The exposed failure surface of the APS sample also indicated an $Y_2Ti_2O_7$ phase, possibly related to the YZTA features identified by SEM/EDS (Figs. 5, 6, 8). At present, it believed that the Zr and Al EDS intensities always associated with these particles do actually correspond to this phase, although no information on a quaternary oxide phase structure was found in the xrd database. These features were often >5 µm and should not reflect background intensity from the surrounding YSZ or Al_2O_3 chemistry. Analysis of the backside (uncoated) surface yielded relative peak intensities of ~3% and 12% for TiO_2 and $TiAl_2O_5$ for the APS samples but only 0.4% and 2% for the PS-PVD sample. This is consistent with the lower weight gain of the latter, and may have resulted from beneficial pre-oxidation effects in the low pO_2 of the PS-PVD chamber (~100 Pa of Ar/He, or 0.001 bar). The primarily Al_2O_3 scales show moderate undulations and thickness variation, especially for the APS coatings. There is little indication of a cyclic instability, such as ratcheting or rumpling. The waviness may be related to the grain structures and anisotropic diffusion along various Ti_2AlC lathes.

4. Discussion

4.1. Comparison to furnace cycle tests for superalloys

The oxidation behavior and failure times of the stepped temperature screening tests above provide some insights regarding potential

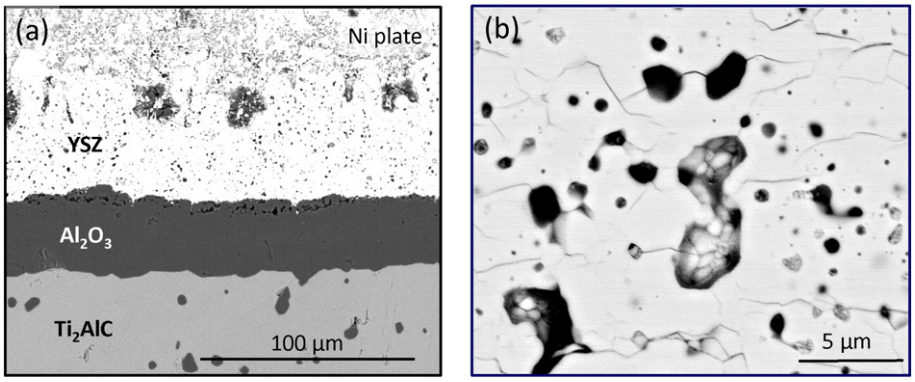

Fig. 11. Cross-section of PS-PVD YSZ–Ti_2AlC interface after 500 h testing at 1300 °C (SEM/BSE). a) Overview showing intact YSZ coating and intact 32–37 µm Al_2O_3 scale; (b) higher magnification of YSZ showing dense network of fine lateral microcracks.

capabilities. For example, it is clear that this TBC oxidative durability was at least on the order or hundreds of hours at 1200 °C, 1250 °C, or 1300 °C. This in itself should be enough to distinguish these systems from conventional metallic systems that generally exhibit these lives at 1150 °C [15]. However the total oxidative life on Ti_2AlC was on the order of 2500 h for these tests, achieving unusually thick thermally grown scales before failure. In order to provide a more direct comparison to typical cyclic tests performed at one temperature, a detailed analysis is presented below. Subsequently, the rationale for this life extension is discussed on the basis of matched coefficients of thermal expansion, with proportionally reduced thermal stress and strain energy factors that control spallation.

4.1.1. Scale thickness at failure

The durability of TBC systems on metallic substrates has often been related to the scale thickness that can be tolerated before failure occurs. This may be a combination of stress concentrations that occur at asperities, debonding at valleys in any ratcheting/rumpling distortion, and increases in strain energy as the scale grows. An empirical value of 7 μm has often been mentioned as a 'critical' scale thickness, x_c, for TBC failure on superalloy substrates [22]. Fig. 12 presents the x_c values mentioned above for the APS and EB-PVD coatings on Ti_2AlC (converted from overall weight gain as ~29 and 35 μm, respectively) in reference to those previously compiled for EB-PVD coatings on bond coated superalloys and bulk NiAl(Zr) [15]. The bond coats include typical Pt-modified aluminides, Pt-only, and NiCoCrAlY overlay coatings and show an average $x_c \sim 6 \pm 2$ μm, essentially agreeing with 7 μm. Coatings on the Ti_2AlC MAX phase survived above 1200 °C, with ~30 μm scale thicknesses, i.e., ~5× that sustained for metal systems.

4.1.2. Comparative oxidative life of YSZ coatings on bulk Ti_2AlC and typical bond coats on superalloys

Here we compare oxidative life between the stepped temperature tests of TBCs on Ti_2AlC with those of conventional furnace cycle tests of TBCs on superalloy systems. The procedure is to calculate the time needed to achieve the appropriate scale thickness observed for a given temperature on each system, which requires some attention to detail. Isothermal TGA tests characterized this Ti_2AlC over 1100–1300 °C [9] and corrected for a measurable amount of TiO_2 transient "knee" in log–log plots, Table 1, now including new data obtained at 1000° and 1400 °C. It is seen that the kinetics are sub-parabolic, with m ranging from 0.24–0.36, and near the reported cubic rate [2,3,9]. The cubic rate

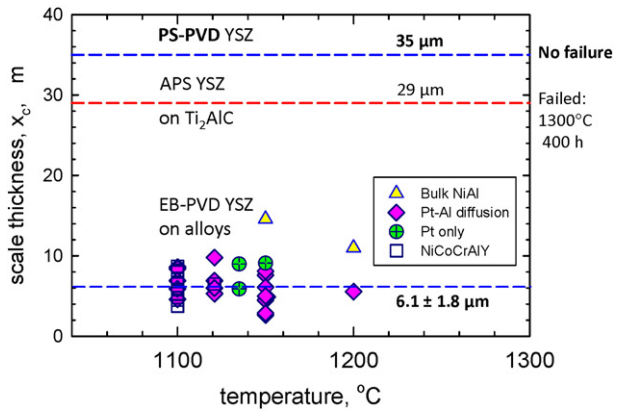

Fig. 12. Minimum scale thickness achieved at failure for YSZ coated Ti_2AlC MAX phase compared to literature values (compiled in ref. [15]) for ~25 EB-PVD coatings on bond coated superalloys and bulk NiAl(Zr). Average scale thickness at failure: 6.1 ± 1.8 μm, with no temperature dependence indicated for any bond coat.

constant, affected by grain growth [2,9,23,24,25], is then determined according to:

$$\left(\frac{\Delta W}{A} - \frac{\Delta W_k}{A}\right)^3 = k_c(t - t_k)$$

from $t^{1/3}$ plots, shown in Table 1 and Fig. 13.

Similarly, isothermal TGA tests of a conventional Ni(Pt)Al coated single crystal superalloy were determined over the 1000–1250 °C temperature range [15], Fig. 14. The projected equivalent times to produce the measured scale thickness on Ti_2AlC are shown in Fig. 15. They significantly exceed the times to achieve the 7 μm boundary corresponding to the upper limit for coated superalloys. Indeed the lives of the MAX phase TBC systems exceeds the superalloy coatings on the order 25–50×. Alternatively, this advantage can be viewed as an increased temperature capability of ~200 °C for the same scale thickness equivalent lifetime. These improvements are considered to result from the close CTE match between YSZ, α-Al_2O_3, and Ti_2AlC as compared to NiAl coatings or superalloy substrates. Other factors for improved life are the lack of coating rumpling caused by CTE mismatch with superalloy substrates. Finally, any instabilities triggered by diffusional losses to the substrate and the rapid creation of Al-depleted phases are precluded in the case of bulk Ti_2AlC substrates which do not generally exhibit a depletion zone.

These positive comparisons may need to be tempered somewhat to account for the thinner TBC layers and lack of frequent 1-h cycling for the present coatings. It can certainly be argued that more typical 250 μm APS and 125 μm YSZ coatings would exhibit reduced cyclic durability than the 100 and 80 μm respective coatings studied here. However these effects are likely to produce less than a 2–5× differential in life, whereas a potential improvement of 50× was indicated. Thicker TBCs may actually experience less average stress than thinner ones (see below). Although a more frequent cycle frequency (e.g., every hour) would seem to decrease durability, no indication of scale decohesion was ever observed. Rapid cycling (8000 cycles to 1350 °C) had been shown to produce no damage to the 15 μm scale formed on similar material [14]. And in another study, scales survived 1000 1-h cycles to 1200 °C [4]. Thus the more likely damage factor would accrue from crack growth in the TBC. This mechanism presented itself primarily in the APS coating after its strain tolerance and toughness had been compromised by sintering or phase separations at 1250 °C and above.

4.1.3. Residual stress and strain energy factor

It is well-recognized that TBC and scale spallation in furnace cycling tests (FCT) are influenced by high thermal expansion mismatch stresses. For example, the CTE of Rene′N5 is ~16.0 ($\times 10^{-6}$/°C) as compared ~8.2 for Ti_2AlC, 9.3 for Al_2O_3 and 11.3 for YSZ [12,26,27]. The CTE measured for Ti_2AlC in the present study was 10.2×10^{-6}/°C over the 700–1300 °C range. Thus, cooling from high temperature will produce a high compressive biaxial stress in the plane of the scale. Such stress in a three-layer system can be estimated from a closed form solution, assuming a semi-infinite slab geometry, a stress-free state at high temperature and no sintering or plastic flow [28,29]. Using the nominal material parameters, geometry, and temperature in Table 2, it is predicted that the compressive stress in the Al_2O_3 scale would be ~−3700 MPa for metallic substrates. This is in the range of values measured by photoluminescence spectroscopy [22]. In contrast, for Ti_2AlC substrates, the stresses in the Al_2O_3 scale would be just −521 MPa (~1/7 that of the metallic system). In addition, over the 1000–1300 °C heating temperatures, the compressive stress in the Al_2O_3 scale is projected to increase from −433 to −566 MPa. Indeed, very similar residual compressive stresses of −360 to −510 MPa were measured by photoluminescence for Al_2O_3 scales grown on a different Ti_2AlC substrate at 1000 °C to 1400 °C for 25 h, with a slightly lower measured CTE (9.6×10^{-6}/°C) [4].

By comparison, the predicted stresses change very little over these ranges in both the Ti_2AlC substrate and YSZ top coat. The corresponding

Table 1
Summary of isothermal oxidation parameters for Ti_2AlC transient knee, log–log slope (m), and k_{cubic} 100 h regression fits (°C, h, mg/cm^2, mg/cm^2/(h)$^{1/3}$ corresponding units).

TGA test	log log knee			log log slope				$t^{1/3}$ fit			
T (°C)	T_k (°C)	t_k (h)	ΔW_k	t_o (h) regr.	$\log\Delta W_{0,log}$	m	r^2	t_o (h) regr	$\Delta W_{0,cubic}$ (mg/cm^2)	k_{cubic}	r^2
1000	856	0.038	0.146	1.0	−0.785	0.235	0.996	1	0.105	0.082	0.993
1100	839	0.028	0.168	0.1	−0.696	0.308	0.999	1	0.057	0.166	1.000
1200	1103	0.037	0.307	0.1	−0.481	0.318	1.000	1	0.017	0.307	1.000
1300	1167	0.058	0.382	0.1	−0.301	0.362	1.000	1	−0.130	0.596	1.000
1400	758	0.022	0.183	1.0	0.103	0.302	0.999	5	0.281	1.008	1.000

stresses in the 100 μm YSZ coating would be ~− 136 MPa for metal and + 54 MPa for Ti_2AlC substrates, respectively. Increasing the YSZ thickness to 500 μm on Ti_2AlC substrates only slightly decreases the stress in YSZ to + 50 MPa.

Also, it has been proposed that a strain energy factor ultimately controls failure of α-Al_2O_3 scales and TBCs that rely on them for interface stability [22,30,31]. That is, once the compressive stored strain energy exceeds the toughness of the scale-substrate interface, the scale is unstable and is energetically favored to debond. Strain energy varies according to the factor $x(\Delta T\Delta\alpha_{CTE,})^2\ (1\text{-}\nu_{Al2O3})^2\ E_{(Al2O3)}$. (where x refers to scale thickness, T temperature, α_{CTE} coefficient of thermal expansion, and E,$\nu_{(Al2O3)}$ bulk modulus and Poisson's ratio) [31]. Thus it can be shown from the parameters in Table 2 that the strain energy in the Al_2O_3 scale formed on a superalloy system at 1150 °C, failing at a scale thickness of 10 μm and strain energy of 175 J/m^2, is projected to be ~12.5 times that for 35 μm scales that survived on the Ti_2AlC MAX phase at 1300 °C, with a strain energy of only 14 J/m^2. This is consistent with the greater FCT lives observed for TBCs on alumina-forming Ti_2AlC substrates.

If the $\Delta\alpha_{CTE}$ for a Ti_2AlC substrate is 1/7 of that of a metal substrate, the induced stresses will be ~1/7 as great. This suggests that less severe failure mechanisms may apply compared to the compressive failure that occurs on metal substrates. Furthermore, high tensile adhesive strengths were measured by epoxied stubs for the α-Al_2O_3 scale-Ti_2AlC interfacial bond, >85 MPa [32], suggesting even greater durability. This corroborates the excellent scale adhesion observed in cyclic tests. These factors both contribute to the excellent scale retention on Ti_2AlC during thermal cycling. While scale thickening will gradually increase the strain energy in the scale upon cooling Ti_2AlC, it is unclear whether this will be accommodated by interfacial debonding, cracking of an adherent scale, or minor deformation at the Ti_2AlC interface.

Failure of the APS coating did not involve interfacial scale spallation to any great extent. The mixed fracture surface appeared to be within the TBC near the scale, within the outer layer of the scale, or exactly at the TBC-scale interface. APS YSZ coatings are well known to sinter, shrink, and increase E_{TBC} and the interfacial shear stress. These may have all been factors that led to failure. Additionally, the YZTA reaction phase may have altered interface compliance and contributed to failure, though it was not omnipresent. The Ti-rich phases, originating from the initial TiO_2 transient layer, did not appear to thicken appreciably from 1200 °C through 1250° and 1300 °C testing (accruing an additional 1000 hot hours), but may still play a role in the final failure mechanism.

Finally, Rietveld analyses revealed a very high ~60% monoclinic content at the end of 1300 °C, 500 h testing, presumably formed on cool down from an equilibrium, phase separated tetragonal. The volume change associated with this transformation is generally believed to weaken and damage the YSZ. Along with sintering shrinkage, this may have played a role in crack growth and failure here, although the spalled flake remained primarily intact as one piece. In comparison, the PS-PVD coating had ~30% monoclinic after 1300 °C, 500 h testing and still survived. The cause of these differences in monoclinic was not investigated, but may be related to different starting powder monoclinic content, powder homogeneity, and process history during melting/vaporization/deposition.

For the PS-PVD coating, a high density of fine, dispersed porosity was displayed within the TBC that apparently retained strain tolerance. Dispersed porosity is known to at least decrease E and thus stress in the TBC. This is one mechanism by which PS-PVD coatings are expected to be more durable and strain-tolerant [20,21]. The polished cross-section displayed only minor amounts of interfacial porosity, minimal cracking, and YZTA reaction phase. While fine cracks were sometimes observed in this coating, they appeared to be much less detrimental than for the APS coating. The alumina scales remained adherent even when the APS coating failure did occur after exposures at very high temperature. Increased porosity within the scale, reactions within the TBC,

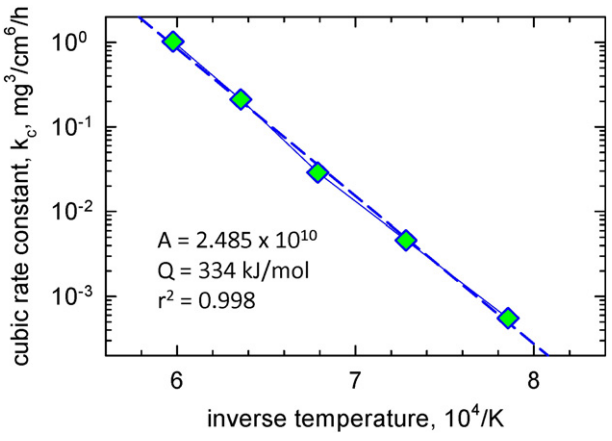

Fig. 13. Temperature dependence of cubic rate constant (k_c) for isothermal oxidation of Ti_2AlC MAX phase. Activation energy from regression fitted line is 334 kJ/mole [9].

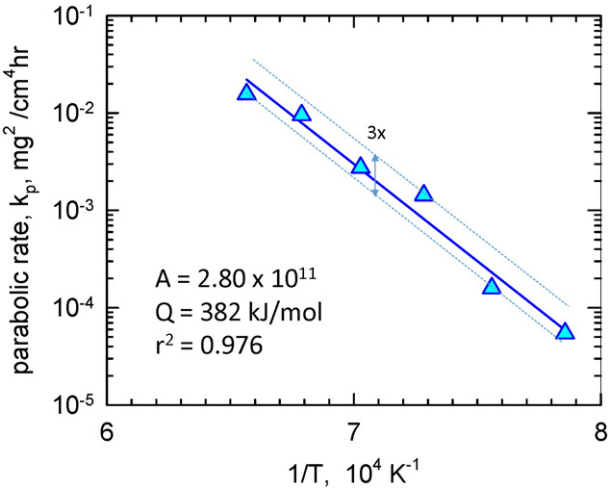

Fig. 14. Temperature dependence of parabolic rate constant (k_p) for isothermal oxidation of Pt-modified aluminide coating on 2nd generation single crystal superalloy [15]. (Dotted lines indicate scatter boundaries). Activation energy from regression fitted line is 382 kJ/mole.

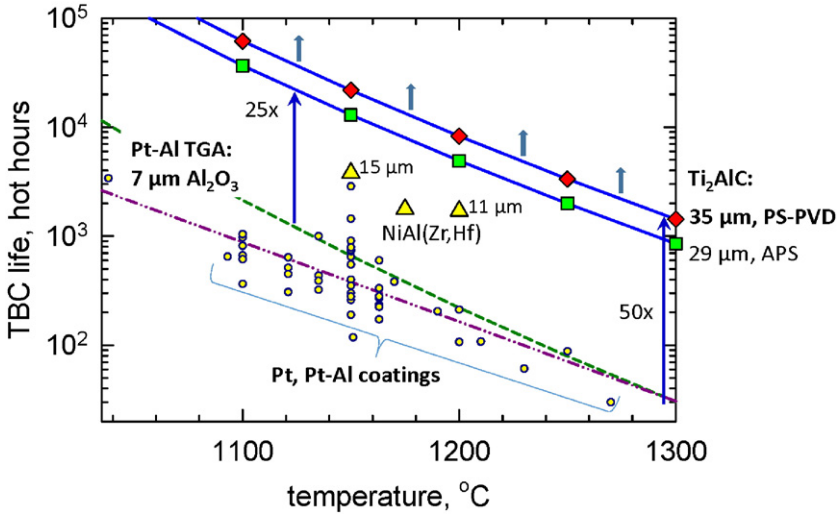

Fig. 15. Comparison of TBC lives on Ti_2AlC with those on metal substrates. Compiled EB-PVD lives for Pt-aluminide and Pt-only coatings on superalloys as a function of temperature [15]. Overall average behavior indicated by regression fit line (dash dot dot). TGA predicted time to grow 7 μm critical thickness of α-Al_2O_3 on metal bond coats (dashed curve). TGA predicted time to grow 29 and 35 μm of α-Al_2O_3 on Ti_2AlC indicated by square (APS) and diamond (PS-PVD) symbols, respectively.

and changes in microstructure are likely to determine life at 1300 °C. Nevertheless, both coatings exhibited remarkable oxidative lives in this first demonstration on MAX phases in successive, intermittent furnace tests.

Thus it is seen that low thermal stresses contribute to the compatibility of YSZ thermal barrier coatings on Ti_2AlC MAX phase substrates, especially in comparison to current metallic superalloy-based systems. The MAX phase system can survive extremely high temperatures and long times because the α-Al_2O_3 scales remain intact for the duration. However this is not meant to imply that a TBC/MAX phase system can be easily substituted for current metallic bond coats or substrates. CTE compatibility, and interdiffusion with superalloys will likely be great obstacles to simple substitution for Ni(Pt)Al bond coats with a Ti_2AlC bond coat. Deposition techniques do not abound for thick coatings that may be needed to capitalize on the CTE matching and stress reduction in the scale and YSZ. Finally, though interesting, the mechanical properties cannot compete with superalloy substrates at temperatures less than 1150 °C. It is suggested that low stress, high heat environments provide the most realistic opportunities for a TBC/MAX phase component. Indeed, component redesign to mitigate these problems and maximize the advantages will most likely be required.

5. Summary and conclusions

This study presented preliminary trials of APS and PS-PVD YSZ TBC coatings on a commercial Ti_2AlC MAX phase compound. No special preparations or process modifications were required, other than a light grit blast. Furnace oxidation durability tests, run in 50 °C increments from 1100–1300 °C for 500 h each, did not visibly degrade the coatings until 1300 °C. Here the APS coating began to pull away at a corner after 15 h and exhibit buckling, failing catastrophically from 400–500 h. The failed sample exhibited a high monoclinic YSZ content (and some cubic) due to destabilization of the as-sprayed metastable t′ tetragonal phase. These TBC microstructures contained large pores and long, wide cracks, with a prominent Y–Zr–Ti–Al oxide reaction phase at the fracture surface. These features and sintering out the compliant splat boundaries at 1200–1300 °C are put forth as the primary factors leading to failure [33]. Subsequent work focused more on the details of the failure mechanism, rather than life testing presented here, appears warranted.

In contrast, the PS-PVD TBC coating remained completely intact through the 1100–1300 °C testing. The degree of monoclinic YSZ was about ½ that found in the APS coating. While some fine interfacial porosity and reaction particles were observed, the primary YSZ layer remained homogeneous, with no large cracks, and compliant with finely dispersed porosity. The fine and uniform microstructural features of this coating and higher retained t′ phase contents are believed to contribute to its superior performance.

No spalling of the alumina scale was observed for either coating for the total test duration. These extended TBC oxidation lives allowed atypically thick α-Al_2O_3 scales to be achieved on Ti_2AlC under the TBC. While conventional bond coats on superalloys have been shown to achieve 6 ± 2 μm of scale on average before TBC failure, these Ti_2AlC systems achieved a minimum of 29 and 35 μm, respectively. Some initial indication of oxidative durability is indicated by the ~2400–2500 h total exposures endured. But a more precise indication of minimum oxidative life was surmised from the times predicted (from TGA kinetics) to achieve equivalent scale thicknesses. Here a relative improvement factor up to 50× in life (or 200 °C ΔT) can be projected. Specifically, ~10,000 h would be needed to achieve the projected survivable 35 μm thick α-Al_2O_3 scale on Ti_2AlC at 1200 °C. This is compared to about 200 h, on average, for TBC failure on Pt-aluminide coated superalloys. Eventually, at very high temperatures, changes within the TBC would likely dominate potential failure mechanisms, defining a finite time/temperature use envelope.

Table 2
Material System Parameters for Thermal Stress Calculations (YSZ top coating, Al_2O_3 scale, and Ti_2AlC or Rene′N5 substrates).

		Units	YSZ	Al_2O_3	Ti_2AlC	N5
E	Young's	GPa	48	400	278	220
a	CTE	1E-6/K	11.7	9.3	10.2	16
n	Poisson		0.1	0.23	0.185	0.33
x	Thickness		100 μm	20 μm	2.08 mm	2.08 mm
T	Temperature	°C	1200	1200	1200	1200
s	Stress	MPa	54	−521	2	N.A.
s	Stress	MPa	−136	−3714	N.A.	35

Acknowledgments

The authors are grateful to D.L. Humphrey for TGA tests, Dereck Johnson for CTE measurements, and to J.A. Buehler for metallographic preparations. This work was funded by the NASA Fundamental Aeronautics Program.

References

[1] M.W. Barsoum, T. El-raghy, the max phases : unique new carbide and nitride materials, Am. Sci. 89 (July–August) (2001) 334–343.
[2] D.J. Tallman, B. Anasori, M.W. Barsoum, A critical review of the oxidation of Ti_2AlC, Ti_3AlC_2 and Cr_2AlC in air, Mater. Res. Lett. 1 (3) (Sep. 2013) 115–125.
[3] X.H. Wang, Y.C. Zhou, High-temperature oxidation behavior of Ti_2AlC in air, Oxid. Met. 59 (2003) 303–320 (April).
[4] J.W. Byeon, J. Liu, M. Hopkins, W. Fischer, N. Garimella, K.B. Park, M.P. Brady, M. Radovic, T. El-Raghy, Y.H. Sohn, Microstructure and residual stress of alumina scale formed on Ti_2AlC at high temperature in air, Oxid. Met. 68 (2007) 97–111.
[5] Z.J. Lin, M.S. Li, J.Y. Wang, Y.C. Zhou, Influence of water vapor on the oxidation behavior of Ti_3AlC_2 and Ti_2AlC, Scr. Mater. 58 (1) (Jan. 2008) 29–32.
[6] S. Basu, N. Obando, A. Gowdy, I. Karaman, M. Radovic, Long-term oxidation of Ti2AlC in air and water vapor at 1000–1300 °C temperature range, J. Electrochem. Soc. 159 (2) (2012) C90.
[7] G.M. Song, V. Schnabel, C. Kwakernaak, S. van der Zwaag, J.M. Schneider, W.G. Sloof, High temperature oxidation behaviour of Ti_2AlC ceramic at 1200 °C, Mater. High Temp. 29 (3) (Aug. 2012) 205–209.
[8] M.W.M. Radovic, Barsoum, MAX phases: bridging the gap between metals and ceramics, Am. Ceram. Soc. Bull. 92 (3 April) (2013) 20–27.
[9] J.L. Smialek, Kinetic aspects of Ti_2AlC MAX phase oxidation, Oxid. Met. 83 (3–4) (2015) 351–366.
[10] J.L. Smialek, Oxygen diffusivity in alumina scales grown on Al-MAX phases, Corros. Sci. 91 (Feb. 2015) 281–286.
[11] X.H. Wang, F.Z. Li, J.X. Chen, Y.C. Zhou, Insights into high temperature oxidation of Al_2O_3-forming Ti_3AlC_2, Corros. Sci. 58 (May 2012) 95–103.
[12] T.H. Scabarozi, S. Amini, O. Leaffer, A. Ganguly, S. Gupta, W. Tambussi, S. Clipper, J.E. Spanier, J.D. Hettinger, S.E. Lofland, T.H. Scabarozi, S. Amini, O. Leaffer, A. Ganguly, S. Gupta, W. Tambussi, Thermal expansion of select M n + 1 A X n (M = early transition metal, A = A group element, X = C or N) phases measured by high temperature X-ray diffraction and dilatometry, J. Appl. Phys. 105 (013543) (2009) 1–9.
[14] M. Sundberg, G. Malmqvist, A. Magnusson, T. El-Raghy, Alumina forming high temperature silicides and carbides, Ceram. Int. 30 (7) (Jan. 2004) 1899–1904.
[15] J.L. Smialek, Compiled furnace cyclic lives of EB-PVD thermal barrier coatings, Surf. Coat. Technol. 276 (2015) 31–38.
[16] B.A. Pint, I.G. Wright, W.Y. Lee, Y. Zhang, K. Prüßner, K.B. Alexander, Substrate and bond coat compositions: factors affecting alumina scale adhesion, Mater. Sci. Eng. A 245 (1998) (1998) 201–211.
[17] B.A. Pint, I.G. Wright, W.J. Brindley, Evaluation of thermal barrier coating systems on novel substrates, J. Therm. Spray Technol. 9 (June) (2000) 198–203.
[18] D. Rigney, R. Darolia, W. Walston, R. Corderman, "'Nickel aluminide coating and coating systems formed therewith', US Patent 6,153,313.," 2000.
[19] B. Hazel, J. Rigney, M. Gorman, B. Boutwell, R. Darolia, Development of improved bond coat for enhanced turbine durability 1, Superalloys 2008 2008, pp. 753–760.
[20] G. Mauer, M.O. Jarligo, S. Rezanka, A. Hospach, R. Vaßen, Surface & coatings technology novel opportunities for thermal spray by PS-PVD, Surf. Coat. Technol. 268 (2015) 52–57.
[21] L. Gao, H. Guo, L. Wei, C. Li, S. Gong, H. Xu, Microstructure and mechanical properties of yttria stabilized zirconia coatings prepared by plasma spray physical vapor deposition, Ceram. Int. 41 (7) (2015) 8305–8311.
[22] V.K. Tolpygo, D.R. Clarke, K.S. Murphy, Oxidation-induced failure of EB-PVD thermal barrier coatings, Surf. Coat. Technol. 146–147 (2001) 124–131.
[23] W.J. Quadakkers, Growth mechanisms of oxide scales on ODS, Werkst. Korros. 41 (1990) 659–668.
[24] D. Naumenko, B. Gleeson, E. Wessel, L. Singheiser, W.J. Quadakkers, Correlation between the microstructure, growth mechanism, and growth kinetics of alumina scales on a FeCrAlY alloy, Metall. Mater. Trans. A 38 (12) (Nov. 2007) 2974–2983.
[25] K. Bongartz, W.J. Quadakkers, J. Pfeifer, J. Becker, Mathematical modelling of oxide growth mechanisms measured by 180 tracer experiments, Surf. Sci. 292 (1993) 196–208.
[26] J. Cheng, E. Jordan, B. Barber, M. Gell, Thermal/residual stress in an electron beam physical vapor deposited thermal barrier coating system, Acta Mater. 46 (16) (1998) 5839–5850.
[27] W. Tian, P. Wang, Y. Kan, G. Zhang, Oxidation behavior of Cr_2AlC ceramics at 1,100 and 1,250 °C, J. Mater. Sci. 43 (8) (Feb. 2008) 2785–2791.
[28] C.H. Hsueh, Thermal stresses in elastic multilayer systems, Thin Solid Films 418 (2) (2002) 182–188.
[29] C.H. Hsueh, L.C. De Jonghe, C.S. Lee, Modeling of thermal stresses in joining two layers with multi- and graded interlayers, J. Am. Ceram. Soc. 89 (1) (2006) 251–257.
[30] A.G. Evans, D.R. Mumm, J.W. Hutchinson, G.H. Meier, F.S. Pettit, Mechanisms controlling the durability of thermal barrier coatings, Prog. Mater. Sci. 46 (2001) 505–553.
[31] H.E. Evans, Oxidation failure of TBC systems: an assessment of mechanisms, Surf. Coat. Technol. 206 (7) (2011) 1512–1521.
[32] Z. Lin, M. Zhuo, Y. Zhou, M. Li, J. Wang, Microstructures and adhesion of the oxide scale formed on titanium aluminum carbide substrates, J. Am. Ceram. Soc. 89 (9) (2006) 2964–2966.
[33] D. Zhu, R.A. Miller, Sintering and creep behavior of plasma-sprayed zirconia- and hafnia-based thermal barrier coatings, Surf. Coat. Technol. 108–109 (1–3) (1998) 114–120.